Advances in Engineering Software 187 (2024) 103566

Contents lists available at ScienceDirect

Advances in Engineering Software

journal homepage: www.elsevier.com/locate/advengsoft

Multi-scale topology optimization of structures with multi-material microstructures using stiffness and mass design criteria

Fábio M. Conde [a,b,*], Pedro G. Coelho [a,b,c], José M. Guedes [b]

[a] UNIDEMI, Department of Mechanical and Industrial Engineering, NOVA School of Science and Technology, Universidade NOVA de Lisboa, 2829-516 Caparica, Portugal
[b] IDMEC, Instituto Superior Técnico, Universidade de Lisboa, Av. Rovisco Pais 1, 1049-001 Lisboa, Portugal
[c] LASI, Intelligent Systems Associate Laboratory, 4800-058 Guimarães, Portugal

ARTICLE INFO

Keywords:
Multi-scale
Multi-material
Composites
Topology
Optimization
Stiffness

ABSTRACT

Nowadays, there is a great interest on the part of the automotive and aerospace industry to design environmentally-friendly structures. To that purpose, stiffness-oriented designs are proposed here by extending previous work on multi-scale topology optimization to the multi-material setting reformulating the problem to include appropriately mass constraints and discussing different design domain parametrizations and algorithmic strategies.

On the macroscale, the problem of minimizing the compliance subject to a global mass constraint is addressed. On the microstructure scale, the multi-material design is carried out by solving the problem of minimizing the local complementary strain energy density with mass density constraint. As a result, very efficient structures composed of spatially varying porous and multi-material microstructures are obtained. The optimal design of the multi-material microstructure can be done either in a pointwise manner or in larger subdomains, to promote design uniformity. These parametrizations are here compared and discussed. Moreover, two different algorithmic strategies to solve the multi-scale problem are proposed, and their pros and cons discussed. They differ in the way the macro and micro design variables are related and updated. The macro design variables consider the mass density distribution along the structure, while the micro variables define the microstructure's topology using a multi-material SIMP interpolation scheme.

The results show very efficient structures with locally optimized multi-material microstructures, which can outperform their single-material counterparts with regards to stiffness while maintaining the same mass. Additionally, the maximum stress verified on multi-material structures tends to be lower than the one obtained in the single-material counterparts.

1. Introduction

The optimization of multi-scale structures is carried out resorting to different design length scales. Typically, two length scales are considered: macroscale and microscale. At the macroscale, the structure is viewed as comprised of a material with microstructure assumed locally periodic. Multi-scale structures can be found in nature, e.g., bone and bamboo, and they hold the promise of achieving superior performance while being intrinsically lightweight, robust and multi-functional [51]. Over the past years, the optimal design of multi-scale structures has received increasing attention mainly due to the rapid developments in Addictive Manufacturing (AM). AM provides an effective means to fabricate optimized multi-scale structures exhibiting in general complex and fine geometrical details. Combining AM with computational design tools, as Topology Optimization (TO), has proved to be a sound approach to design and materialize multi-scale structures [28,30].

Topology Optimization has been widely used in the mechanical, automotive, and aerospace industries since the original work of Bendsøe and Kichuchi [6]. Several methods to perform TO have been proposed so far, such as the density-based approach [5], Level-Set [50], Topological Derivative [43] and Phase Field [7]. The vast majority of contributions on TO relate to single-scale structural design (see [18]), while comparatively few address multi-scale design [51]. However, multi-scale structures compared to single-scale structures have the potential to

Submitted to Advances in Engineering Software
* Corresponding author.
E-mail addresses: f.conde@campus.fct.unl.pt (F.M. Conde), pgc@fct.unl.pt (P.G. Coelho), jmguedes@tecnico.ulisboa.pt (J.M. Guedes).

https://doi.org/10.1016/j.advengsoft.2023.103566
Received 29 June 2023; Received in revised form 20 October 2023; Accepted 22 November 2023
Available online 3 December 2023

excel in performance, motivating research on the multi-scale topic.

Multi-scale TO, also known in the literature as hierarchical TO, has a pioneer contribution from Rodrigues et al. [40], where the structure and material (microstructure) are concurrently optimized. This involves two material models at different length scales, and also two different optimization problems to be solved, one for each length scale. The global (or macro) problem determines the optimal macroscopic spatial distribution of homogenized material, while the local (or micro) problem is actually a set of optimization problems responsible for determining the optimal microscopic spatial distribution of base materials and void phases at each macro design point. The original bidimensional hierarchical model by Rodrigues et al. [40] was later extended to three dimensions by Coelho et al. [11], and then the computer implementation was parallelized by Coelho et al. [10]. Afterwards, Coelho and Rodrigues [12] suggested a different parametrization for the macro-domain considering larger design subdomains, grouping several finite elements of the global mesh, in order to reduce the total number of problem design variables, i.e., avoiding an element-by-element design. A different multi-scale optimization approach able to reproduce comparable results but using level sets was introduced by Sivapuram et al. [42]. In the attempt of improving the manufacturability of multi-scale structures, Liu et al. [37] proposed an interpolation scheme on the macro-scale known as Porous Anisotropic Material with Penalization (PAMP). The objective with such interpolation scheme is to obtain "gray–white" designs easy to manufacture. The manufacturability is an important issue when designing multi-scale structures. Therefore, the geometrical compatibility of adjacent material microstructures is also a concern that has been addressed by the research community (see e.g., [19,31,36,48,59] and [24]).

Bringing together multi-material and multi-scale design approaches can open even more the design space to search for optimal structural solutions exceling in performance. Multi-Material Topology Optimization (MMTO) consists in designing a structure composed of two or more solid material phases. To perform MMTO using a density-based method, a suitable interpolation scheme must be chosen. The classical SIMP method can be extended to interpolate more than two solid phases, so-called Recursive SIMP, see Bendsøe and Sigmund [3]. Other interpolation schemes have been proposed, see e.g.: Discrete Material Optimization (DMO) in Stegmann and Lund [44]; Shape Function with Penalization (SFP) in Bruyneel [9] and James [26]; Peak Function in Yin and Ananthasuresh [53]; and ordered SIMP in Zuo and Saitou [60]. Besides these schemes for density-based MMTO problems, there are also other ones to solve multi-material problems using the level-set [22,49] and phase field methods [47,58]. The vast majority of the works perform MMTO in single-scale structures, most of them on the macroscale (see, e.g., [35] and [32]) and only a few on the microscale (see, e.g., [13]). MMTO has been applied to multi-scale structures in a much less extent as summed up below.

To the authors' knowledge, the first work where structure and material are concurrently designed using MMTO techniques is Xu et al. [52]. In that work, the composite macrostructure and periodic microstructure with multi-phase materials are concurrently optimized using the so-called Bi-Directional Evolutionary Structural Optimization (BESO) method [25]. The objective is to minimize the dynamic compliance of the macro structure under harmonic excitation force. Later, Jia et al. [27] presents a hierarchical TO method to simultaneously achieve the optimal structures and multiphase material unit-cells that minimize the system thermal compliance. Only one finite element model is considered, where the structure and material unit-cell are coupled through elemental phase relative density, skipping the homogenization method. Afterwards, Da et al. [16] carries out optimization for composite structures and the underlying multi-phase materials simultaneously. It considers a macrostructure made of two periodic composites, each one has three or more phase materials. There are three finite element models, one macro model for the macrostructure and two micro models for the material representative unit-cells. The objective is to minimize the structural compliance (or maximize the structural stiffness). The same authors extended their work for thermal conductivity in Da et al. [15], where the objective is to minimize the overall structural thermal compliance. In Zhang et al. [55] the authors performed a multi-scale TO, aiming for improved stiffness, applied to cellular multi-material structures. At the macroscale, a density-based TO is solved using the order SIMP interpolation scheme to find out the optimal overall structure layout with multiple materials. At the microscale, a parametric level set method is applied to evolve the shape and topology of the representative microstructures in each macroscale element. In Liang and Du [34] a concurrent multi-scale and multi-material topological optimization of vibro-acoustic structures for minimizing sound radiation is performed, where an interpolation model based on SIMP and PAMP is developed. Another work that performs multi-scale MMTO is Li et al. [33] with the intend of minimize the dynamic compliance. The macrostructure is composed of uniform multiphase composites with periodic microstructures. Level set functions are used to describe the boundaries of the macrostructure and multiphase microstructure. Applied to heat transfer problems, the work of Pizzolato et al. [39] performs multi-scale MMTO where the layout at the macro-scale is described by level-set fields and the micro-scale geometry is represented through a density approach. More recently, Zhao et al. [56] proposes a concurrent topology optimization method of macrostructural material distribution and periodic microstructure considering dynamic stress response under random excitations. The optimization problem is the minimization of the dynamic stress response of the macrostructure subject to volume constraints in both macrostructure and microstructure. Ultimately, Costa et al. [14] proposes a two-scale concurrent optimization of lattice structure, where surrogate models are used to represent material and geometrical properties for a continuous topology optimization approach. Despite the several contributions on multi-scale MMTO pointed out so far, none of them extends the original hierarchical problem proposed by Rodrigues et al. [40] to the multi-material setting, which is here done considering mass constraints and a different optimization algorithm. On the one hand, the aforementioned research works assume a macrostructure composed of a single (or a few) composite material(s), whose microstructure and location within the macroscopic design domain are concurrently optimized. The present work, on the other hand, intents the local optimization of the periodic multi-phase material within the macrostructure aiming for extremely efficient structures in terms of trade-off between stiffness and lightweight design criteria. Moreover, the majority of contributions in stiffness-oriented multiscale MMTO consider volume constraints instead of mass constraints. The advantage of having mass constraints in stiffness-oriented MMTO is that the presence of different material phases is not enforced unlike multi-material formulations based on material volume fraction constraints.

In this work, the multi-scale MMTO is formulated for the structural compliance minimization problem, where the objective is to minimize the global compliance (or maximize the global stiffness) of a cellular structure while subject to a mass constraint. Here, the multi-material design model is applied to the microscale design domain (unit-cell). The ultimate goal is to design structures, with multi-material microstructures, that have enhanced performance when compared to their single-material counterparts of the same mass. As previously mentioned, the multi-scale problem combines a global design problem with a set of local design problems. The global and local problems can be coupled, and different algorithmic strategies and design parameterizations can be used to obtain a solution. Two of these strategies and parametrizations are considered in the present work. Regarding the algorithmic strategies, they define how the global and local design variables are related. The global design variables (macro-densities) can be either implicitly or explicitly computed from the local design variables (micro-densities), thus giving rise to two distinct categories of algorithmic strategies: (1) *implicit*; and (2) *non-implicit*. As regards the design parametrizations, these define how the macrostructure is to be optimized. The

macrostructure can be either optimized in a pointwise fashion, where each material point of the structure is locally optimized, or in larger subdomains, where microstructural design uniformity is assumed within each subdomain. These two algorithmic strategies and design parameterizations are explored and compared here in the framework of multi-scale MMTO, as it has not been reported in the literature, to the best of authors' knowledge.

This paper is outlined as follows. In Section 2 the macroscale and microscale material models are presented. Afterwards, one formulates the multi-scale MMTO problem, derives the necessary conditions for optimality and performs a sensitivity analysis in Section 3. The methodology behind the multi-scale optimization, including a detailed explanation of the aforementioned algorithmic strategies and design parameterizations, can be found in Section 4. In Section 5 one presents the obtained results solving the multi-scale MMTO problem using the different approaches studied. Finally, the main conclusions of this work are presented in Section 6.

2. Material model

The material model used here is two dimensional and comprises two length scales, the macroscale (structure domain, Ω) and the microscale (microstructure domain, ¥), see Fig. 1. At the macroscale level, one is interested in defining the distribution of a cellular/composite material across the structure design domain, Ω. Whereas at the microscale level, the focus is on the design of a unit-cell viewed as the smallest representative heterogeneity of the periodic cellular/composite material from which the structure is made of. In the present framework, one designs microstructures that can be made up of one or two different base materials (plus void). Both local periodicity and separation of length scales are assumed, i.e., the microstructure is periodic throughout the structure domain and has a feature size much smaller than the global size of the structure. Bearing this in mind, the homogenization method [23] can be conveniently applied. By applying the homogenization method, it is possible to treat a heterogeneous medium as a homogeneous one, i.e., with equivalent or homogenized mechanical properties.

2.1. Macroscale model

The macroscale model considered here has two different boundary conditions applied, a displacement boundary condition ∂u and a load-based boundary condition ∂F, where plane stress is assumed, see Fig. 1. The equilibrium problem is solved numerically resorting to the Finite Element Method (FEM), where the original FEM2D Fortran code developed by Kikuchi [29] is adapted here to use the 8-node quadrilateral elements (Q8), which prevents shear-locking.

The structure design domain Ω can be divided into several design subdomains Ω_i and inside each one the material microstructure is assumed uniform, i.e., only one local problem needs to be solved within each Ω_i. Although the material design freedom is reduced as the size of these design subdomains increases, the continuity/connectivity of material microstructures across the structure domain becomes a lesser issue than considering smaller design subdomains. Furthermore, these enlarged design domains reduce the total number of problem design variables, thus the computational cost too, and it also reduces the spatial variation of properties, turning manufacturability easier. In stark contrast, an increased design freedom, on account of decreasing the design subdomains' size may imply that, ultimately, each design subdomain could be as small as the single FE size. This actually recovers the most natural way to perform multi-scale TO, where each macro-FE is associated with the design of a porous/composite material therein. This means, at a macroscopic level, an element-by-element definition of an optimal material microstructure. This kind of parametrization leads to the solution of a very high number of local problems across the whole structure domain, which especially appeals to parallel computing to reduce the computational cost. These two different design model parametrizations are covered in the present work. In the first design model each design subdomain Ω_i is comprised of several FEs, i.e., $\Omega_e \subset \Omega_i$. In the second one, each design subdomain coincides with the FE size Ω_e, i.e., $\Omega_e \equiv \Omega_i$.

The several design subdomains correspond to periodic material media with microstructure, and the material properties of each one are computed through homogenization resorting to the analysis of a representative Unit-Cell (UC). The microstructures are assumed to have a number of material phases up to two (plus void). Details about the

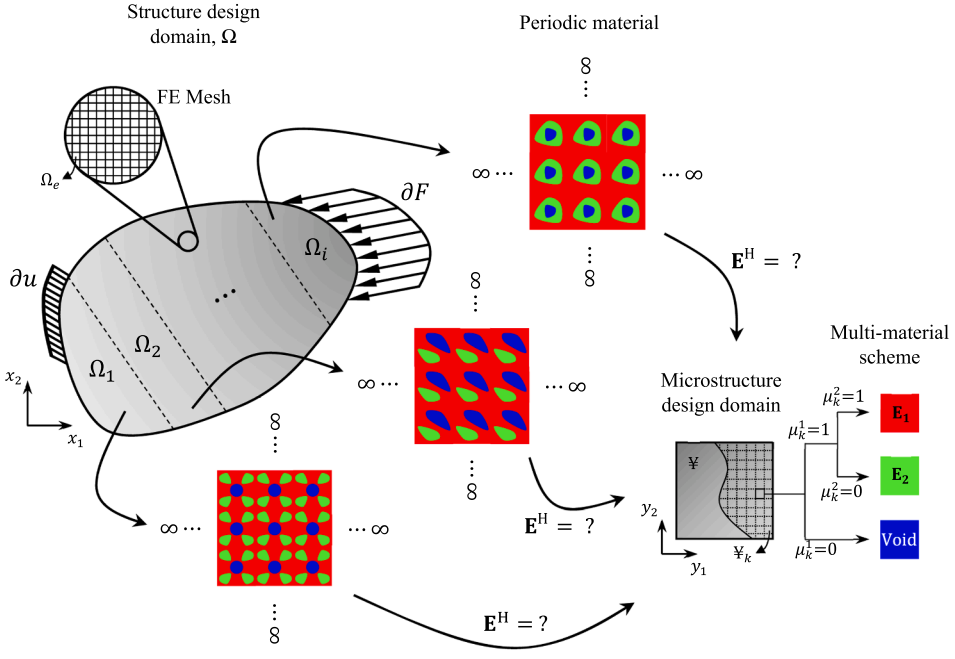

Fig. 1. Multi-scale material model description. The structure design domain Ω is divided into *i* design subdomains Ω_i. Each design subdomain has a unique periodic material whose microstructure ¥ can be designed with 2 materials plus void.

microscale model are given in the next section, where the homogenization method and the multi-material interpolation scheme are briefly introduced.

2.2. Microscale model

The equivalent or homogenized stiffness tensor $\mathbf{E}^{\mathrm{H}}$ in each Ω_i is predicted using the asymptotic homogenization method [21]:

$$E^{\mathrm{H}}_{ijkl} = \frac{1}{|¥|}\int_{¥} E_{pqrs}\left(\delta_{rk}\delta_{sl} - \frac{\partial \chi^{kl}_r}{\partial y_s}\right)\left(\delta_{pi}\delta_{qj} - \frac{\partial \chi^{ij}_p}{\partial y_q}\right) \mathrm{d}¥ \tag{1}$$

where $|¥|$ is the unitary UC volume (or area in 2D), $\mathbf{E}$ is the base material stiffness tensor, $\mathbf{y}$ is the position vector defined in ¥, $\boldsymbol{\delta}$ is the Kronecker delta and $\boldsymbol{\chi}$ are the micro-displacements solution of the following problem defined in ¥, comprised by a set of three equilibrium equations (in 2D):

$$\int_{¥} E_{ijrs}\frac{\partial \chi^{kl}_r}{\partial y_s}\frac{\partial v_i}{\partial y_j}\,\mathrm{d}¥ = \int_{¥} E_{ijkl}\frac{\partial v_i}{\partial y_j}\,\mathrm{d}¥, \forall\ \mathbf{v} \in ¥ - \text{periodic} \tag{2}$$

The base material stiffness tensor $\mathbf{E}$ at a given point in the microstructure is given by the SIMP-based multi-material interpolation law [3], which depends on the micro design variables $\boldsymbol{\mu}^1$ and $\boldsymbol{\mu}^2$:

$$E_{pqrs} = \left(\mu^1\right)^{p_1}\left[\left(\mu^2\right)^{p_2}E^1_{pqrs} + \left(1-\left(\mu^2\right)^{p_2}\right)E^2_{pqrs}\right] \tag{3}$$

where $\mu^1, \mu^2 \in [\mu_{min}, 1]$ with $\mu_{min} = 10^{-3}$ to prevent singularity issues; $\mathbf{E}_1$ and $\mathbf{E}_2$ are the stiffness tensors of the solid phases (with $\mathbf{E}_1 > \mathbf{E}_2$); and p_1, $p_2 \geq 3$ are the penalization exponents that disfavour intermediate density values of μ^1 and μ^2 in compliance-based problems [4]. In this interpolation scheme, the design variable μ^1 works as a topological variable as it identifies presence or absence of the solid phase, and the design variable μ^2 is responsible for the material selection ($\mathbf{E}^1$ or $\mathbf{E}^2$), see Fig. 1(d). The multi-material interpolation law in Eq. (3) could be extended to interpolate among an increased number of materials by simply adding terms, so-called Recursive SIMP. However, the SIMP-based interpolation scheme has been claimed unsuitable when applied to more than three phases [44]. In that case, DMO could be more recommended. Since in this study one interpolates between two solids plus void, SIMP works just fine.

The stresses $\boldsymbol{\sigma}$ in the microstructure can be computed based on the applied average macroscopic strain tensor $\langle\boldsymbol{\varepsilon}\rangle$ through:

$$\sigma_{ij} = E_{ijrs}\left(\delta_{rk}\delta_{sl} - \frac{\partial \chi^{kl}_r}{\partial y_s}\right)\langle\varepsilon_{kl}\rangle \tag{4}$$

The applied average macroscopic strain tensor $\langle\boldsymbol{\varepsilon}\rangle$ can be related with the applied average macroscopic stress tensor $\langle\boldsymbol{\sigma}\rangle$ as:

$$\langle\varepsilon_{rs}\rangle = C^{H}_{rspq}\langle\sigma_{pq}\rangle \tag{5}$$

where $\mathbf{C}^{\mathrm{H}}$ is the homogenized compliance tensor, computed as the inverse of the homogenized stiffness tensor $\mathbf{E}^{\mathrm{H}}$, such that:

$$E^{\mathrm{H}}_{ijmn}C^{\mathrm{H}}_{mnkl} = \frac{1}{2}\left(\delta_{ik}\delta_{jl} + \delta_{il}\delta_{jk}\right) \tag{6}$$

The FEM is used to solve Eqs. (1), (2) and (4) numerically, see PREMAT and POSTMAT Fortran Subroutines in Guedes and Kikuchi [21]. The domain ¥ is discretised into a square-grid mesh with 4-node isoparametric finite elements.

3. Multi-scale optimization framework

The multi-scale optimization in the present framework aims to concurrently optimize the distribution of cellular material within the macrostructure design domain, while optimizing the topology and mixture of two materials plus void inside the cellular material design domain. Therefore, each scale has dedicated design variables as formulated in the next section.

3.1. Problem formulation

In this work, one proposes the following multi-scale MMTO problem formulation based on compliance minimization, assuming structures comprised of periodic multi-material microstructures, subject to a mass constraint:

$$\underset{\rho}{min}\ \ \frac{1}{2}\sum_i^{n_i}[\phi_i(\rho_i,\mathbf{u})|\Omega_i|] \tag{7.1}$$

$$\text{s.t.}\quad \sum_i^{n_i}[\rho_i|\Omega_i|] - M^* \leq 0 \tag{7.2}$$

$$0 < \rho_{\min} \leq \boldsymbol{\rho} \leq \rho_{\max} \leq \overline{\rho}_1 \tag{7.3}$$

where $\mathbf{u}$ is the unique solution of the equilibrium equations (minimizer of the total potential energy) found by the FEM2D program, $|\Omega_i|$ is the volume (area in 2D) of the subdomain i, and ϕ_i is the minimum "energy density" found in the subdomain i, given by:

$$\phi_i(\rho_i,\mathbf{u}) = \min_{\boldsymbol{\mu}^1,\boldsymbol{\mu}^2}\ \mathbf{C}^{\mathrm{H}}\left(\tilde{\boldsymbol{\mu}}^1,\tilde{\boldsymbol{\mu}}^2\right)\frac{\int_{\Omega_i}\boldsymbol{\sigma}(\mathbf{u})\boldsymbol{\sigma}(\mathbf{u})\mathrm{d}\Omega_i}{|\Omega_i|} \tag{8.1}$$

$$\text{s.t.}\quad \sum_k^{n_k}\left[\tilde{\mu}^1_k\left(\tilde{\mu}^2_k\overline{\rho}_1 + \left(1-\tilde{\mu}^2_k\right)\overline{\rho}_2\right)|¥_k|\right] - \rho_i|¥| \leq 0 \tag{8.2}$$

$$\frac{\sum_k^{n_k}\left[\tilde{\mu}^1_k\left(1-\tilde{\mu}^2_k\right)|¥_k|\right]}{|¥|} - V^*_2 \leq 0 \tag{8.3}$$

$$0 < \mu_{\min} \leq \boldsymbol{\mu}^1 \leq 1 \tag{8.4}$$

$$0 < \mu_{\min} \leq \boldsymbol{\mu}^2 \leq 1 \tag{8.5}$$

where the set of equations (7) states the TO problem of the macrostructure design, while the set of equations (8) states the TO problem of the microstructure design. The macro TO problem aims the minimization of the total strain energy given by (7.1), where n_i is the total number of design subdomains Ω_i. The design variable $\boldsymbol{\rho}$ is a vector containing the mass densities (i.e., mass per unit volume) ρ_i of all subdomains Ω_i, and must not be confused with the dimensionless (artificial) density variable typically used in classical TO. The global mass constraint (7.2) ensures that the structure's mass is not beyond its maximum allowable value M^*. This mass limit value is defined according to the global mass density bounds such that $M^* \in [\rho_{\min}|\Omega|, \rho_{\max}|\Omega|]$, where $|\Omega|$ is the structure design domain volume (area in 2D). The lower and upper bounds of the macro design variables are $\rho_{\min}$ and $\rho_{\max}$, respectively. As regards the micro TO problem, it aims the local minimization of the complementary strain energy density of the material design domain Ω_i (8.1) while subject to a local mass constraint (8.2), where n_k is the total number of micro-FEs, $\overline{\rho}_1$ and $\overline{\rho}_2$ are the mass densities of the stiffer and weaker solids, respectively. This local mass constraint relates the macro and micro design variables and therefore is supposed to be an equality constraint, but due to practical issues involving the optimizer, an inequality constraint is used instead. Since a compliance minimization problem is solved here, this local constraint is active or nearly active along design iterations. To correctly model and optimize multi-material microstructures composed of three material phases, two micro design variables $\boldsymbol{\mu}^1$ and $\boldsymbol{\mu}^2$ are required. In contrast to the macro problem, these design variables are standard densities varying from 0 (or a very small number $\mu_{\min}$) to 1, see (8.4) and (8.5). To avoid numerical problems, such as checkerboard patterns and mesh dependence, a density-based

filtering technique is used here (see [8]). While this technique is applied to both micro design variables, $\boldsymbol{\mu}^1$ and $\boldsymbol{\mu}^2$,the macro design variable, $\boldsymbol{\rho}$, is left unfiltered. Thereafter, the corresponding filtered micro densities, $\tilde{\boldsymbol{\mu}}^1$ and $\tilde{\boldsymbol{\mu}}^2$, are the ones really defining the UC layout, while original design variables, $\boldsymbol{\mu}^1$ and $\boldsymbol{\mu}^2$, have no physical meaning. The additional constraint on the local volume fraction of the weaker material in (8.3) is an artifice to always ensure defined $\boldsymbol{\phi}$ derivatives as explained later in Section 4.

3.2. Optimality conditions

To obtain the necessary conditions for the proposed multiscale design problem, the Lagrangian function for each problem, macro and micro, must be defined. The Lagrange function associated with the macro problem (7) at points where $\boldsymbol{\rho}$ takes intermediate values (i.e., side constraints are inactive) is given by:

$$\mathscr{L} = \frac{1}{2}\sum_{i}^{n_i}[\phi_i(\rho_i,\mathbf{u})|\Omega_i|] + \Lambda\left(\sum_{i}^{n_i}[\rho_i|\Omega_i|] - M^*\right) \tag{9}$$

where $\Lambda \geq 0$ is the Lagrange multiplier associated with the global mass (inequality) constraint. The stationarity of the Lagrange function $\mathscr{L}$ defined above with respect to (w.r.t.) the design variable $\boldsymbol{\rho}$ is given by:

$$\frac{\partial \mathscr{L}}{\partial \boldsymbol{\rho}} = 0 \Leftrightarrow \frac{1}{2}\frac{\partial \phi_i}{\partial \rho_i}|\Omega_i| = -\Lambda|\Omega_i| \Leftrightarrow \frac{\partial \phi_i}{\partial \rho_i} = -2\Lambda \tag{10}$$

In design points where the constraint on the volume fraction of the weaker solid (8.3) and design variables side constraints (8.4 and 8.5) are inactive, the Lagrange function of the micro problem (8) can be written as:

$$\ell_i = \mathbf{C}^{\mathrm{H}}\frac{\int_{\Omega_i}\boldsymbol{\sigma}\boldsymbol{\sigma}\mathrm{d}\Omega_i}{|\Omega_i|} + \lambda_i\left(\sum_{k}^{n_k}\left[\tilde{\mu}_k^1\left(\tilde{\mu}_k^2\overline{\rho}_1 + \left(1-\tilde{\mu}_k^2\right)\overline{\rho}_2\right)|¥_k|\right] - \rho_i|¥|\right) \tag{11}$$

where $\boldsymbol{\lambda}$ is the Lagrange multiplier of the local mass constraint. The stationary of the Lagrange function ℓ w.r.t. both filtered design variables $\tilde{\boldsymbol{\mu}}^1$ and $\tilde{\boldsymbol{\mu}}^2$ is given by:

$$\frac{\partial \ell_i}{\partial \tilde{\mu}_k^1} = 0 \Leftrightarrow \frac{\partial \mathbf{C}^{\mathrm{H}}}{\partial \tilde{\mu}_k^1}\frac{\int_{\Omega_i}\boldsymbol{\sigma}\boldsymbol{\sigma}\mathrm{d}\Omega_i}{|\Omega_i|} = -\lambda_i\left(\tilde{\mu}_k^2\overline{\rho}_1 + \left(1-\tilde{\mu}_k^2\right)\overline{\rho}_2\right)|¥_k| \tag{12}$$

$$\frac{\partial \ell_i}{\partial \tilde{\mu}_k^2} = 0 \Leftrightarrow \frac{\partial \mathbf{C}^{\mathrm{H}}}{\partial \tilde{\mu}_k^2}\frac{\int_{\Omega_i}\boldsymbol{\sigma}\boldsymbol{\sigma}\mathrm{d}\Omega_i}{|\Omega_i|} = -\lambda_i\left(\tilde{\mu}_k^1\overline{\rho}_1 - \tilde{\mu}_k^1\overline{\rho}_2\right)|¥_k| \tag{13}$$

Note that the macro stresses $\boldsymbol{\sigma}$ do not depend on the micro density fields when solving the micro problem because these stresses are prescribed by the macro problem analysis and then used as constants at the micro problem level.

Using the sensitivity theorem (see e.g., [20]) to relate the macro and micro Lagrange multipliers, one can rewrite the necessary condition (10) as follows:

$$\frac{\partial \phi_i}{\partial \rho_i} = -\lambda_i \Leftrightarrow \lambda_i = 2\Lambda \tag{14}$$

3.3. Sensitivity analysis

This work uses the Method of Moving Asymptotes (MMA, [45]) as the optimizer to solve the multi-scale optimization problem. Since this is a gradient-based optimizer, one needs to perform sensitivity analysis.

Since one uses the density filtering technique, the sensitivities of the objective and constraint functions w.r.t. a density design variable, $\boldsymbol{\mu}$, are computed based on the respective filtered density derivative through the application of the chain rule (see [41]):

$$\frac{\mathrm{d}f}{\mathrm{d}\mu_k} = \sum_{i\in N_k}\frac{\partial f}{\partial \tilde{\mu}_i}\frac{\mathrm{d}\tilde{\mu}_i}{\mathrm{d}\mu_k} = \sum_{i\in N_k}\frac{\partial f}{\partial \tilde{\mu}_i}\left[\frac{R_{min} - \| y_k - y_i \|}{\sum_{j\in N_k}\max\{0, R_{min} - \| y_k - y_i \|\}}\right] \tag{15}$$

where f is a general function, index k refers to the micro finite element k, N_k defines the respective set of elements neighbouring element k, the norm $\|y_k - y_i\|$ sets the spatial distance between elements i and k centroids, and R_{min} is the filter radius.

The objective and constraint functions of the macro (F and G, respectively) and micro (f and g, respectively) problems have the derivatives presented in Table 1.

4. Methodology

This section details the methodology employed to perform multi-scale MMTO using two different algorithmic strategies: (1) *implicit* and (2) *non-implicit*. The advantages and disadvantages of each one will be discussed here. In a nutshell, the *implicit* strategy assumes that the macro mass density field is implicitly computed through the micro densities, which are set as independent design variables, while the *non-implicit* strategy assumes both densities, macro and micro, as independent design variables.

In the *implicit* strategy, the maximization of the global strain energy is entirely done on account of the micro density field update. This simplifies the algorithm as it means solving all the micro problems at once. The prior cascade statement, equations (7) and (8), can be replaced by the following equivalent compact optimization problem statement:

$$\min_{\mu_{i,k}^1,\,\mu_{i,k}^2} \quad \frac{1}{2}\int_{\Omega}\mathbf{C}^{\mathrm{H}}\boldsymbol{\sigma}\boldsymbol{\sigma}\mathrm{d}\Omega \tag{16.1}$$

$$\text{s.t.} \quad \sum_{i}^{n_i}\overbrace{\left[\frac{\sum_{k}^{n_k}\left[\tilde{\mu}_{i,k}^1\left(\tilde{\mu}_{i,k}^2\overline{\rho}_1 + \left(1-\tilde{\mu}_{i,k}^2\right)\overline{\rho}_2\right)|¥_k|\right]}{|¥|}|\Omega_i|\right]}^{\rho_i} - M^* \leq 0 \tag{16.2}$$

$$0 < \mu_{\min} \leq \mu_{i,k}^1 \leq 1 \tag{16.3}$$

Table 1
Objective and constraint functions of the multi-scale optimization problem with the corresponding derivatives w.r.t. macro and micro (filtered) design variables, $\boldsymbol{\rho}$ and $\tilde{\boldsymbol{\mu}}$, respectively.

	Macro problem	Micro Problem
Objective Function	$F = \frac{1}{2}\sum_i^{n_i}[\phi_i(\rho_i,\mathbf{u})\|\Omega_i\|]$	$f = \mathbf{C}^{\mathrm{H}}\frac{\int_{\Omega_i}\boldsymbol{\sigma}\boldsymbol{\sigma}\mathrm{d}\Omega_i}{\|\Omega_i\|}$
	$\frac{\mathrm{d}F}{\mathrm{d}\rho_i} = -\frac{1}{2}\lambda_i\|\Omega_i\|$	$\frac{\mathrm{d}f}{\mathrm{d}\tilde{\mu}_k^1} = \frac{\partial \mathbf{C}^{\mathrm{H}}}{\partial \tilde{\mu}_k^1}\frac{\int_{\Omega_i}\boldsymbol{\sigma}\boldsymbol{\sigma}\mathrm{d}\Omega_i}{\|\Omega_i\|}$
		$\frac{\mathrm{d}f}{\mathrm{d}\tilde{\mu}_k^2} = \frac{\partial \mathbf{C}^{\mathrm{H}}}{\partial \tilde{\mu}_k^2}\frac{\int_{\Omega_i}\boldsymbol{\sigma}\boldsymbol{\sigma}\mathrm{d}\Omega_i}{\|\Omega_i\|}$
Constraint functions	$G = \sum_i^{n_i}[\rho_i\|\Omega_i\|] - M^*$	$g_1 = \sum_k^{n_k}[\tilde{\mu}_k^1(\tilde{\mu}_k^2\overline{\rho}_1 + (1-\tilde{\mu}_k^2)\overline{\rho}_2)\|¥_k\|] - \rho_i\|¥\|$
	$\frac{\mathrm{d}G}{\mathrm{d}\rho_i} = \|\Omega_i\|$	$g_2 = \frac{\sum_k^{n_k}[\tilde{\mu}_k^1(1-\tilde{\mu}_k^2)\|¥_k\|]}{¥} - V_2^*$
		$\frac{\mathrm{d}g_1}{\mathrm{d}\tilde{\mu}_k^1} = (\tilde{\mu}_k^2\overline{\rho}_1 + (1-\tilde{\mu}_k^2)\overline{\rho}_2)\|¥_k\|$
		$\frac{\mathrm{d}g_1}{\mathrm{d}\tilde{\mu}_k^2} = (\tilde{\mu}_k^1\overline{\rho}_1 - \tilde{\mu}_k^1\overline{\rho}_2)\|¥_k\|$
		$\frac{\mathrm{d}g_2}{\mathrm{d}\tilde{\mu}_k^1} = \frac{(1-\tilde{\mu}_k^2)\|¥_k\|}{\|¥\|}$
		$\frac{\mathrm{d}g_2}{\mathrm{d}\tilde{\mu}_k^2} = \frac{-\tilde{\mu}_k^1\|¥_k\|}{\|¥\|}$

$$0 < \mu_{\min} \leq \mu_{i,k}^2 \leq 1 \tag{16.4}$$

where n_i is the total number of macro design subdomains, which may represent either a pointwise mass density variation or extended regions of uniform mass density depending on the defined design domain parameterization. Note also that the design variables $\boldsymbol{\mu}^1$ and $\boldsymbol{\mu}^2$ vary in the macro domain Ω (index i), and in the micro domain ¥ (index k). This encloses the hierarchical structure of the optimization problem formulation (16). The problem is solved resorting to MMA as the optimizer, and the algorithm implemented here in Fortran programming language is detailed in Fig. 2(a). The algorithm starts by generating an initial micro design, which is assumed the same at each macro design subdomain i, followed by the application of density filtering. Since the microstructure at this stage is unique across the entire design domain Ω, the homogenization subroutine just needs to be called once. This subroutine provides the initial homogenized compliance ($\mathbf{C}_0^{\mathrm{H}}$) tensor and its corresponding derivatives w.r.t. the filtered micro densities, $\tilde{\boldsymbol{\mu}}$. Remember that the chain rule must be applied afterwards to obtain the objective and constraint functions derivatives w.r.t. the non-filtered densities, $\boldsymbol{\mu}$, sent to the optimizer. This algorithm has two main loops. The outer loop runs the macro-FE model and the optimizer (MMA), until the convergence criterion is met (e.g., maximum number of iterations). At each outer loop iteration, another loop (inner loop) spans all the local design problems to calculate the new homogenized elastic properties

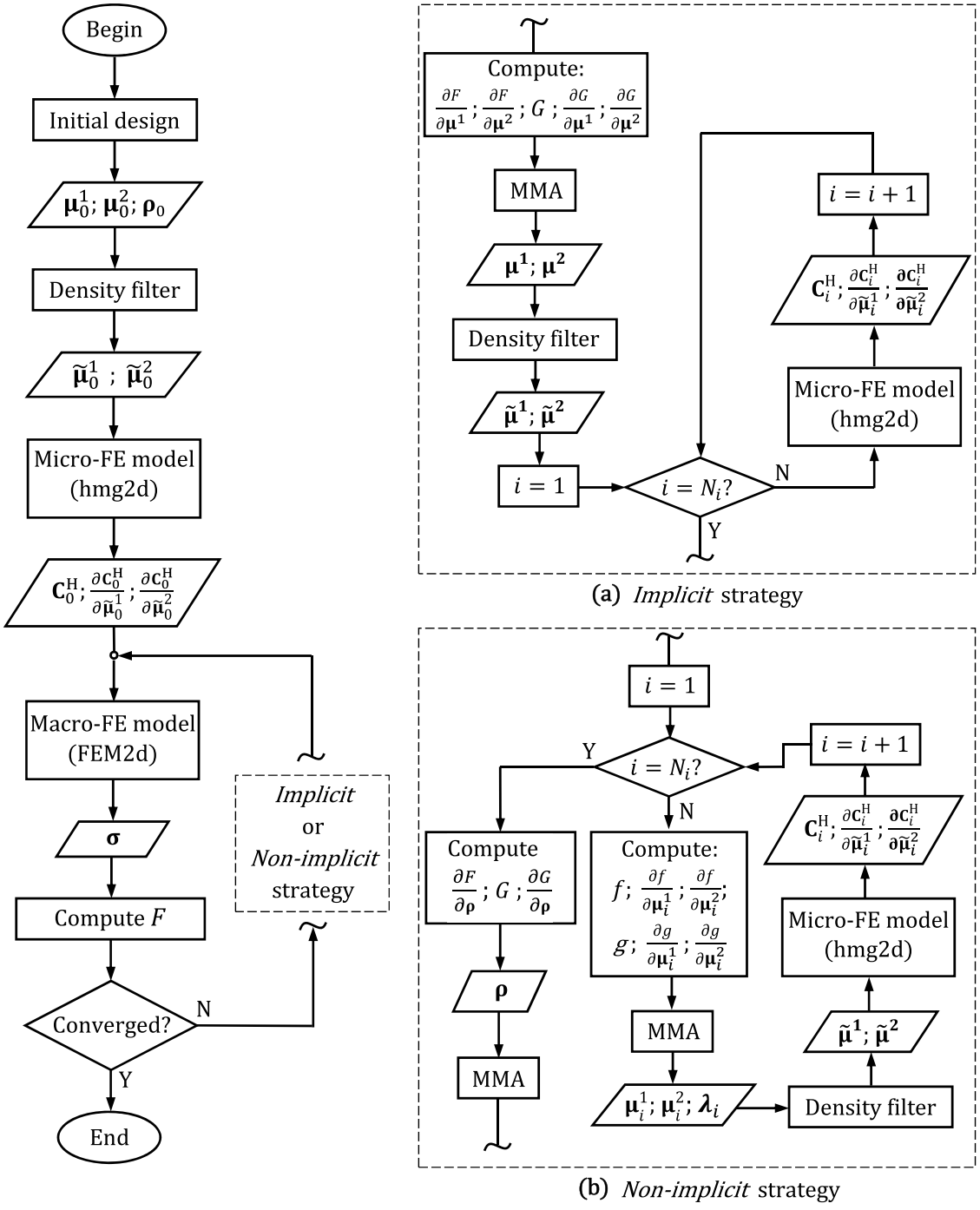

Fig. 2. Flowchart of the algorithm to perform multi-scale optimization considering: (a) an implicit strategy; and (b) a non-implicit strategy.

and corresponding derivatives.

The *non-implicit* strategy naturally handles the hierarchical problem structure as stated by equations (7) and (8), where the two presented optimization problems, each one at a different length-scale, are properly coupled and concurrently solved using two optimizers, one for each scale. Here, MMA can be selected as the optimizer for each scale. Such strategy increases the algorithm complexity and raises convergence issues comparing to the *implicit* strategy. In fact, there are a few key factors to consider for this strategy to work smoothly, that will be discussed later in this section. The algorithm flowchart as regards the *non-implicit* strategy is presented in Fig. 2(b). Similar to the *implicit* strategy, this algorithm also starts with an initialization procedure to set the initial design variables (filtered and non-filtered) and the initial homogenized compliance tensor ($\mathbf{C}_0^{\mathrm{H}}$) along with its derivatives. Two main loops can be identified in the flowchart. The outer loop optimizes the mass density distribution ($\boldsymbol{\rho}$) in the macrostructure, while the inner loop locally optimizes the topology and material distribution of the microstructure (through $\boldsymbol{\mu}^1$ and $\boldsymbol{\mu}^2$) in each macro subdomain Ω_i. Only one MMA design iteration is performed in the inner loop per outer loop iteration in order to avoid premature convergence issues. The outer loop runs until the convergence criterion is verified.

The *non-implicit* algorithmic strategy requires some careful parameter choices for the sake of attaining desired problem convergence. Regarding the micro density design variables, $\boldsymbol{\mu}_i^1$ and $\boldsymbol{\mu}_i^2$, one must ensure that at least one entry or value of each density vector, for each local problem *i*, does not touch its lower or upper bound for the sake of Lagrangian multiplier λ_i existence, which is related to the local mass constraint and calculated by MMA. Otherwise, the Lagrangian multiplier λ_i will be incorrectly defined and, consequently, the objective function derivative, dependent on the functional ϕ_i given by (14), is also incorrect which misleads the gradient-based optimization algorithm on the search for the local minima. Interestingly, the density filter helps overcoming this multiplier non-existence issue because it always ensures some "gray", i.e., $\boldsymbol{\mu}^1$ and $\boldsymbol{\mu}^2$ take some intermediate values. Even so, in the global problem, the mass density variable $\boldsymbol{\rho}$ may touch its bounds, i.e., $\rho_{\min}$ or $\rho_{\max}$, which may become an issue. Notice that in case of selecting side constraints as $\rho_{\min} = \mu_{\min}\,\overline{\rho}_1$ or $\rho_{\max} = \overline{\rho}_1$, the micro densities, $\boldsymbol{\mu}^1$ and $\boldsymbol{\mu}^2$, would be enforced to touch their bounds, $(\boldsymbol{\mu}^1 = \mu_{\min} \wedge \boldsymbol{\mu}^2 = 1) \vee (\boldsymbol{\mu}^1 = 1 \wedge \boldsymbol{\mu}^2 = 1)$, respectively, to verify (8.2). To prevent this from happening, one considers bounds for $\boldsymbol{\rho}$ slightly modified, i.e., $\rho_{\min} = \mu_{\min}\,\overline{\rho}_1 + \zeta$ and $\rho_{\max} = \overline{\rho}_1 - \zeta$, where ζ is a small positive number (e.g., $\zeta = 0{,}00001$ is used here). These slightly adapted bounds can be seen as just what it is needed in the single material setting, see e.g., Coelho and Rodrigues [12]. However, in the bi-material setting, one also realizes another situation where $\boldsymbol{\mu}^1$ and $\boldsymbol{\mu}^2$might be forced to touch their bounds. This is when the microstructure is uniform to represent the weaker solid, i.e., $\boldsymbol{\mu}^1 = 1 \wedge \boldsymbol{\mu}^2 = \mu_{\min}$. A clever way to prevent again $\boldsymbol{\mu}$ from coinciding to the bounds is to constrain the volume fraction of the weaker solid such that it can never be unity. This is the rationale behind using the weaker material volume constraint (8.3), where a limit slightly lower than 1 is used, e.g., $V_2^* = 0.99$. In general, this approach would require one additional local constraint per each solid phase added to the problem. In case more than three material phases are considered, it can be used a single porosity constraint instead of multiple material volume fraction constraints. Although such an approach allows proper calculation of the local Lagrangian multipliers, as provided by MMA, it means that a solid material design solution (microstructure absence) is actually never truly solid or uniform since at least a few intermediate micro density values are enforced. While this tiny density field perturbations do not have any impact on purely compliance-based problems, they prevent stress field distributions from being absolutely uniform as it would be expected for solid microstructures. Later, results shown in Section 5 make this point clearer.

Another relevant issue is the optimizer version of MMA used here to solve the multi-scale problem. It is advisable to use a variant of MMA so-called Generalized Method of Moving Asymptotes (GMMA) proposed by Zhang et al. [54]. The main difference between this version and the original MMA version of Svanberg [45] is that, in GMMA, each design variable x_j in each function $\widetilde{f}_i$ is associated with its proper moving asymptote, L_{ij} (lower one) or U_{ij}(upper one), in order to improve the approximation quality. For example, the two asymptotes can be largely relaxed for linear functions and tightened for nonlinear ones. To solve the multi-scale problem (7–8) or (16) is advisable to have, on one hand, a convex approximation of the compliance function (non-linear) based on moving asymptotes, that can be easily tightened. On the other hand, a linear approximation of the volume/mass constraints is wanted by setting the lower and upper asymptotes to zero and "infinity", respectively. In the problem formulation, note that the constraint functions are linear w.r.t. each design variable (i.e., bilinear functions), meaning that the aforementioned GMMA approximation is exact.

In fact, the asymptotes play an important role in the problem convergence properties, especially when implementing the *non-implicit* strategy. Both global and local optimization problems use MMA as optimizer. However, the parameters and history involved on the asymptotes update scheme are not treated the same way in both problems. In the global problem, such update scheme used to approximate the global strain energy objective function follows the original (default) methodology as proposed by Svanberg [45], where data from previous iterations is used to set up the current asymptotes. This indeed helps the global problem convergence. However, such approach is unsuitable to solve the local problems since only one MMA iteration is performed per global iteration. Using the data from previous local problems (history) proved to give convergence problems according to the authors' experience. Therefore, to improve algorithm's convergence, a continuation approach on the parameter γ_0 (GHINIT variable in MMA Fortran version), that controls the distance between the lower and upper asymptotes, is suggested for the local problem, i.e., its value may decrease along iterations. This ensures that, as the algorithm converges to the optimum, the approximation of the strain energy density function (local problem objective function) becomes more conservative and, consequently, more accurate.

The MMA move limits that keep under control the design variables changes (jumps) is also a sensitive issue when implementing the *non-implicit* strategy. To attain stable convergence, it is important to tighten those move limits for the global design variables while relaxing the variation of those limits for the local design variables. To sum up, move limits should be close to each other when solving the global problem, and apart from each other when solving the local problems. This procedure favors the local mass constraint (8.2) feasibility, avoiding sudden jumps on the related Lagrangian multipliers $\boldsymbol{\lambda}$ as estimated by MMA. The parameter that controls the distance between the move limits is the so-called ALBEFA in the MMA Fortran version. A high ALBEFA value means tightening move limits and vice-versa.

Finally, the algorithm running time may also become an important issue due to many local problems. To address this, parallel computing can be conveniently applied to speedup computations in large-scale problems. For an algorithm to be highly scalable, a coarse-grain parallelism is more desirable than a fine-grain parallelism. In other words, the more individual tasks being parallelized simultaneously, the better. That is the reason why the *non-implicit* strategy is far more attractive to develop parallel code than the *implicit* strategy. Comparing the flowchart in Fig. 2(a) (*implicit* strategy) with the one in Fig. 2(b) (*non-implicit* strategy) helps understanding just that. The inner loop suitable for parallelization in the *implicit* strategy comprehends just the micro-FE analysis, while in the *non-implicit* strategy besides this FE analysis, one also runs the local optimizer in the inner loop. In the former case, MMA deals with one high-dimensional optimization problem since all micro design variables (a huge number) is sent to the optimizer at once, which is quite time-consuming to be treated by MMA. Despite the MMA itself could be parallelized (see [13] and [1]), the scalability compared to the

non-implicit strategy would still be inevitably worse. In the latter case, the local problems are independent (separate) from each other, which is appealing to be tackled by different processors in parallel (e.g., see [10]). The hardware used in this work is a shared-memory Workstation HP Z8 G4, 2 CPUs Intel Xeon 6242R 3.1 GHz 2933 MHz 20C, 256 GB RAM. Since this machine uses shared memory, OpenMP [17] is used to parallelize the code unlike the author's prior parallel code implementation based on MPI [10]. Furthermore, one uses recent available programming Fortran compilers as freeware software provided by Intel®, i.e., OneAPI Base and HPC Toolkits.

5. Results

For the sake of example and synthesis, the different aspects of the proposed methodology for multi-scale MMTO, as the *implicit* and *non-implicit* strategies and the different sizes of design subdomains, are tested using a unique benchmark, the cantilever beam, discretized with 8-node isoparametric FE and assuming plane stress. On one end of the beam, a displacement boundary condition ∂u is applied, where all degrees of freedom are constrained. On the opposite end of the beam, a force-based boundary condition ∂F is applied, where forces are distributed along the edge to avoid stress singularities, see Fig. 3(a). Two different design parametrizations are considered, as shown in Fig. 3(b). On one hand, Fig. 3(b) top, each design subdomain Ω_i contains a couple of layers that are located at opposite sides towards the beam neutral axis. Each layer comprises a row of consecutive FE in the horizontal, x_1, direction. Comprehensively, the total number of layers depends on the number of FEs in the vertical, x_2, direction, and the number of design subdomains halves that total. On the other hand, Fig. 3(b) bottom, each design subdomain has the size of each FE, $|\Omega_e|$, in the mesh.

The level of mesh discretization used in the FE models for the macrostructure and microstructures must be carefully addressed to balance between accuracy and computational cost. Notice that per iteration on the macro design problem, the number of local problems to solve depends on the macro model discretization and parametrization. Taking this into account, the macro and micro design domains are discretised into 50×20 and 100×100 square-FE mesh, respectively. The authors realize that this level of refinement produces accurate results within a reasonable runtime, which is concluded after running a few simulations spanning different discretizations.

The material properties (E and $\overline{\rho}$) considered for the solid material phases are presented in Table 2, where the values of their ratios (in bold) are the ones considered as problem data, instead of the absolute values for the Steel and Aluminium indicated. In fact, the solutions obtained are valid for any two materials that combined present the same E and $\overline{\rho}$ ratios. A Poisson ratio of 0.3 is assumed for both solids.

For comparison purposes only, the multiscale TO problem is also solved for the single-material case, considering only steel as the base material. The idea is to investigate about an improvement on structural stiffness on account of adding one more solid phase (weaker) to the material selection pool while maintaining the same mass threshold in the optimal design problem. The additional solid phase thought here is Aluminium, more compliant but lighter than Steel. Interestingly, the ratio of Young Modulus, between Aluminium and Steel, is basically equal to the ratio of mass density $\overline{\rho}$, which is actually typical of engineering alloys [2].

Table 2
Material properties of Steel (stiffer solid) and Aluminium (weaker solid). Property ratios highlighted in bold.

Materials	E [GPa]	E/E_{Steel}	$\overline{\rho}$ [kg/m^3]	$\overline{\rho}/\overline{\rho}_{\text{Steel}}$
Steel	200	**1**	7900	**1**
Aluminium	68	**0.34**	2700	**0.34**

It is well known that the optima found when solving a non-linear optimization problem using a gradient-based optimizer highly depends on the initial design chosen. Therefore, it is rather important to try out some different initial designs. The generation of initial designs adopted here is always the same. The whole beam is initially composed by the same square-shape microstructure defined with intermediate densities, see Fig. 3(c) for SMTO or Fig. 3(d) for MMTO, such that the total mass threshold M^* is satisfied. Different values of intermediate micro densities defined according to Fig. 3 are tested. Another thing that impacts the optimal solution obtained is the value of exponents p_1 and p_2, and how they change along design iterations. Applying a continuation approach such that $p_1 = p_2 = 2 \rightarrow 4$ during the first global iterations proves to be beneficial, resulting in well-defined binary-like solutions (so-called "black-white" designs). The number iterations needed for the continuation approach vary from case to case. Typically, 40 iterations are enough.

The results are presented below in different sections depending on the macro design parametrization used. Firstly, one considers the *Layer-by-Layer* (LbL) parametrization in Section 5.1 and then the *Element-by-Element* (EbE) parametrization in Section 5.2. In the LbL parametrization, the mass density of each pair of layers located around the middle (neutral) axis of the beam is the macro design variable. In the EbE parametrization each FE contains a design variable which is computationally much more expensive. Therefore, the *implicit* and *non-implicit* strategies, previously described in Section 4, are investigated for the LbL parametrization only, see Sections 5.1.1 and 5.1.2, respectively. Comprehensively, the same investigation is skipped here for the EbE parametrization as it would involve a prohibitive number of design variables (say millions). As mentioned before, the *implicit* strategy is not as appealing as the *non-implicit* one to benefit from speed-ups running the code in parallel, which discourages its usage for the EbE parametrization.

All results shown later consider the same values for the mass threshold, $M^* = 0.3 \times |\Omega|$. Furthermore, the distributed load considers

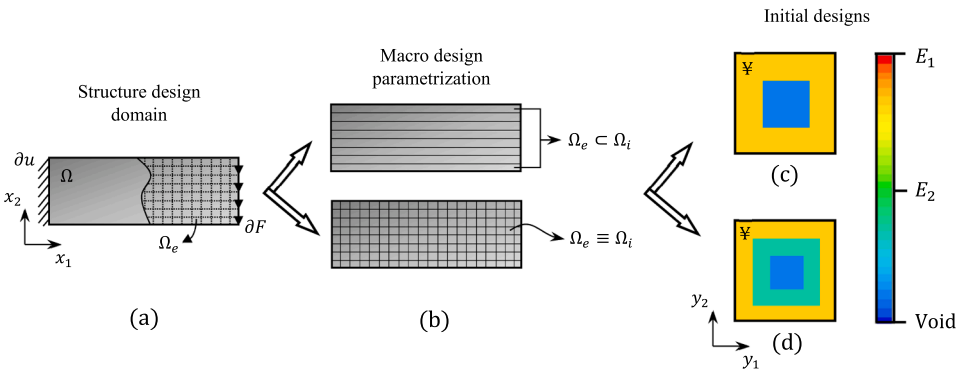

Fig. 3. Multi-scale model applied to a cantilever beam: (a) the structure design domain Ω; (b) two different macroscopic design parametrizations; (c) initial design considered for SMTO; and (d) initial design considered for MMTO.

an applied force of 500 N in all nodes of the beam's right end edge, exception made for the uppermost and lowermost nodes (non-shared nodes) where a force of 250 N is applied instead.

5.1. Layer-by-Layer

This section shows the results obtained solving the multiscale problem using both the *implicit* (Section 5.1.1) and *non-implicit* (Sections 5.1.2) strategies. The *implicit* strategy is used to solve the multiscale problem in both single-material and multi-material settings. For the sake of brevity, the SMTO is skipped for the *non-implicit* strategy since the multi-material optimal solution can already be compared with the single-material solution obtained through the *implicit* strategy.

Besides presenting the optimal mass density distribution on the macrostructure with the corresponding optimal microstructures, one also performs a stress analysis on both scales to enrich and discuss the results. Recall that design symmetry about the neutral axis of the beam is imposed when using the LbL parametrization. To show results, one takes advantage of this symmetry. The upper half of the beam (above the neutral axis) displays the optimal mass density of each layer and the respective material microstructure within it. On the lower half (below the neutral axis), the corresponding von Mises stresses are plotted. Since stresses are not uniform along the layer length, one chooses the "worst-case scenario", i.e., the most stressed finite element in a layer (or subset of layers characterized by the same microstructure), to plot the distribution of stresses in the microstructure. Note that the colour scale for stress changes with the microstructure.

5.1.1. Implicit strategy

The *implicit* strategy implies solving the multiscale problem according to formulation (16). The single and multi-material optimal solutions are presented in Fig. 4 and Fig. 5, respectively, where the micro designs are shown including some stress plots. Further performance comparisons are presented in Table 3.

A beam under bending has normal stresses (higher away from the neutral axis) and shear stresses (higher at the neutral axis). The obtained results are just consistent with that. The mass density $\boldsymbol{\rho}$ decreases from the extreme layers, where laminates and solids better cope with normal stresses, to the neutral axis, where pure cross-shaped microstructures are shear resistant (see e.g., [38,46]). The multi-material optimal solution is 12% stiffer than the single-material one, having both material solutions the same weight. Such increased stiffness is obtained at the expense of an increased material volume fraction, see Table 3, which is also apparent from visual inspection. Observe from Fig. 4 and Fig. 5 that, in MMTO, full solid material solutions are obtained for layers 10 to 7, while in SMTO only layer 10 is solid. Besides that, the cross-shaped microstructures obtained in MMTO are thicker than those obtained in SMTO.

5.1.2. Non-implicit strategy

The multiscale MMTO problem formulated in (7) and (8) is now solved using the *non-implicit* strategy. The optimal solution obtained is presented in Fig. 6, and in Table 3 a comparison with multiscale SMTO and MMTO (*implicit* strategy) is summarized on the basis of energy and stress measures.

Using the *non-implicit* strategy, the algorithm converges to a slightly different multi-material solution compared to the *implicit* strategy. For instance, differences can be observed in layer 9, comparing Fig. 5 and Fig. 6, where the later result shows a microstructure that not only mixes the two solids but also presents void. Despite differences in design, the results obtained using both strategies have similar energy and stress performances. Recall that, in order to have defined derivatives for the macro-problem objective function, one must always ensure some "grey" in the microstructures as previously explained in Section 4 for the *non-implicit* strategy. Therefore, pure single-material design solutions are not obtained with this strategy, i.e., there is always some residual "grey", see microstructures of layers 7 and 8 in Fig. 6. Layer 10 in the vicinity also contains some grey, but it is not perceived from visual inspection since the $\boldsymbol{\rho}$ upper bound is set very close to $\overline{\rho}_1$. This strategy could not be used for layers 7 and 8, where specifically constraint (8.3) plays the role of assuring residual "grey" for the weaker solid solution by setting V_2^* slightly lower than one. In fact, the total strain energy value obtained via the *non-implicit* strategy is always comparatively higher, see Table 3, due to the fact that the single-phase (solid) UC never corresponds to a full distribution of density 1.

Interestingly, the maximum stress value attained in the multi-material solution is lower than the one verified in the single-material case, which is here a mere finding without explicitly introducing stress as a design criterion. As future work it would be also important to include stresses in the optimization problem formulation as objective or constraint. For now, it is possible to anticipate that due to the enforced "grey" presence in single-phase microstructures, a perturbation on the stress field arises, which is an aspect to be given careful attention when elaborating on stress-based formulations.

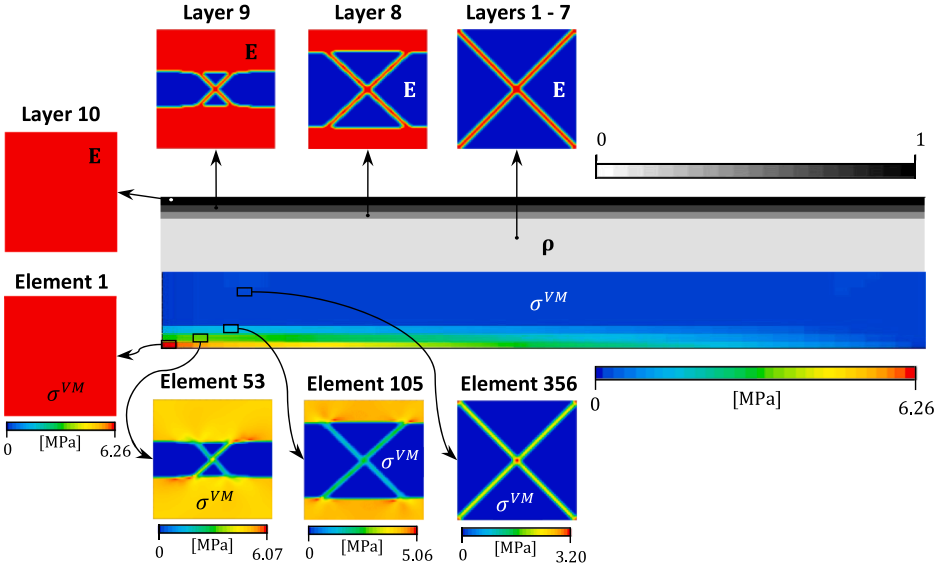

Fig. 4. LbL parametrization and implicit strategy (multiscale SMTO). Optimal mass density $\boldsymbol{\rho}$ distribution along with the optimal single material microstructures (upper half), including Von Mises stress maps (lower half).

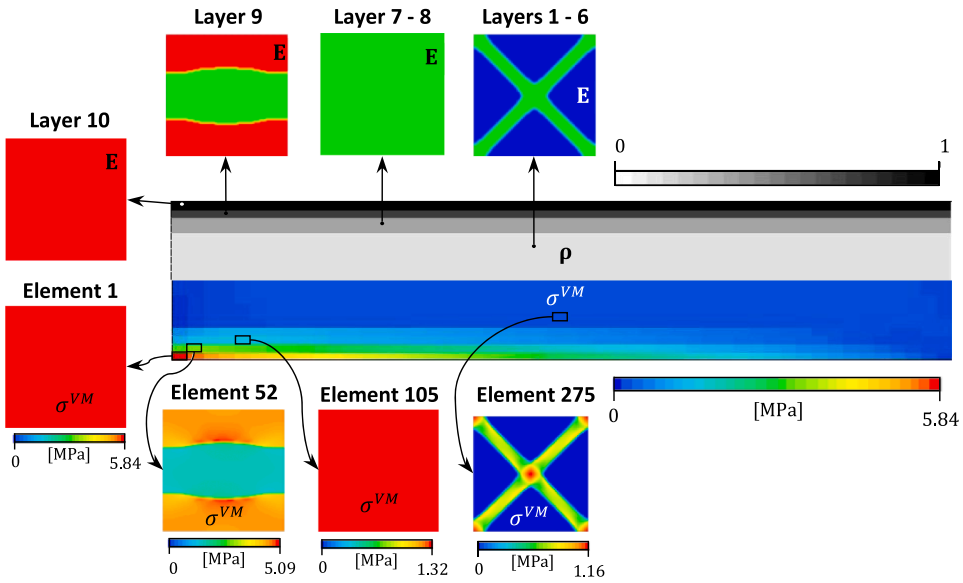

Fig. 5. LbL parametrization and implicit strategy (multi-scale MMTO). Optimal mass density **ρ** distribution along with the optimal multi-material microstructures (upper half), including Von Mises stress maps (lower half).

Table 3
Results obtained using the LbL parametrization, where C^* stands for the total strain energy [J], V^* is the total material volume fraction and σ^{VM}_{max} is the maximum Von-Mises stress in the structure [MPa]. The relative increase or decrease of energy and stress in MMTO compared to SMTO (δ_{SMTO}) is also presented.

	Implicit SMTO	MMTO (δ_{SMTO})	Non-implicit MMTO (δ_{SMTO})
C^*	255.58	224.57 (−12%)	226.92 (−11%)
V^*	0.30	0.57 (+90%)	0.56 (+87%)
σ^{VM}_{max}	6.26	5.84 (−6.7%)	5.83 (−6.9%)

5.2. Element-by-Element

In this section, a similar study as the one performed in the previous section is carried out to compare the performance of single-material designs with multi-material ones. However, such study now considers the EbE parametrization and uses only the *non-implicit* strategy to solve the multiscale problem stated in (7) and (8). Here, the material microstructure may vary among the finite elements as all are design elements, which makes it difficult to show all the obtained material designs. Hence, only a few representative ones are presented. Note that symmetry about the beam neutral axis is not imposed although it is known to be expected. The optimal single-material and multi-material design solutions are presented in Fig. 7 and Fig. 8, respectively. Table 4 compares the total strain energy, material volume fraction and stress values between these solutions. Moreover, the optimization history for the total strain energy and density **ρ** values is provided in Fig. 9 for both solutions.

The higher design freedom given by the EbE parametrization compared to the LbL parametrization explains its superior performance although the lack of design uniformity is an issue when it comes to manufacturability. Microstructural connectivity among adjacent design elements may not be guaranteed here since no method is here used to explicitly impose it. Although the application of such a method is beyond the scope of the present work, it is noteworthy the fact that the literature reports several of such methods, see e.g., Wang et al. [48], Du et al. [19], Li et al. [31], Zhou et al. [59], Liu et al. [36] and Hu et al. [24]. Their application here can be seen as part of an interesting future development. These methods limit the design performance on account of additional problem design constraints. An alternative way to facilitate the connectivity among adjacent microstructures is considering larger design subdomains, which is done here in the setting of the LbL parametrization. However, the LbL parametrization itself decreases design freedom compromising performance. By comparing Table 3 and Table 4, one concludes that the LbL multi-material solution performs worse than the EbE single-material solution. Note that design finite elements symmetric about the neutral axis show symmetrical material designs as expected (see Elements 75 and 925 in Fig. 7), unlike the previous results for the LbL parameterization where symmetrical layers toward the neutral axis are grouped to share the same design.

Comparing the SMTO and MMTO results, benefits in stiffness and strength can be recognized for the same mass requirement using the multi-material and multi-scale design approach, see Table 4. The optimization history presented in Fig. 9 shows a smooth convergence in both cases.

6. Conclusion

The design of multi-scale structures with improved performance, when compared to single-scale counterparts, is a current and growing research topic. With the recent advances in AM technology, the production of complex structural parts as rendered by multi-scale design tools is becoming a reality. Combining multi-scale with multi-material design techniques is a great way to explore outstanding structural performance levels. Acknowledging that, the present framework is a contribution to the state-of-the-art in multiscale MMTO. The authors extend here the work previously developed by Rodrigues et al. [40] to the multi-material setting, focusing on the particular aspects regarding the optimization problem formulation and methodology.

Two different material models are required here to perform TO on multiscale structures, entailing two length scales. The structure at the macroscale is subject to force and displacement boundary conditions, and its spatial variation of material properties depends on the material microstructure, whose design domain is defined at the microscale, assumed locally periodic. Two different design domain parameterizations are considered in the present framework, to characterize how the material microstructure varies across the structure domain. It can either vary pointwisely or remain uniform within enlarged subdomains. The main goal of this work is to perform TO on both scales, concurrently, to find the stiffest structure given a total mass threshold. Therefore, at the

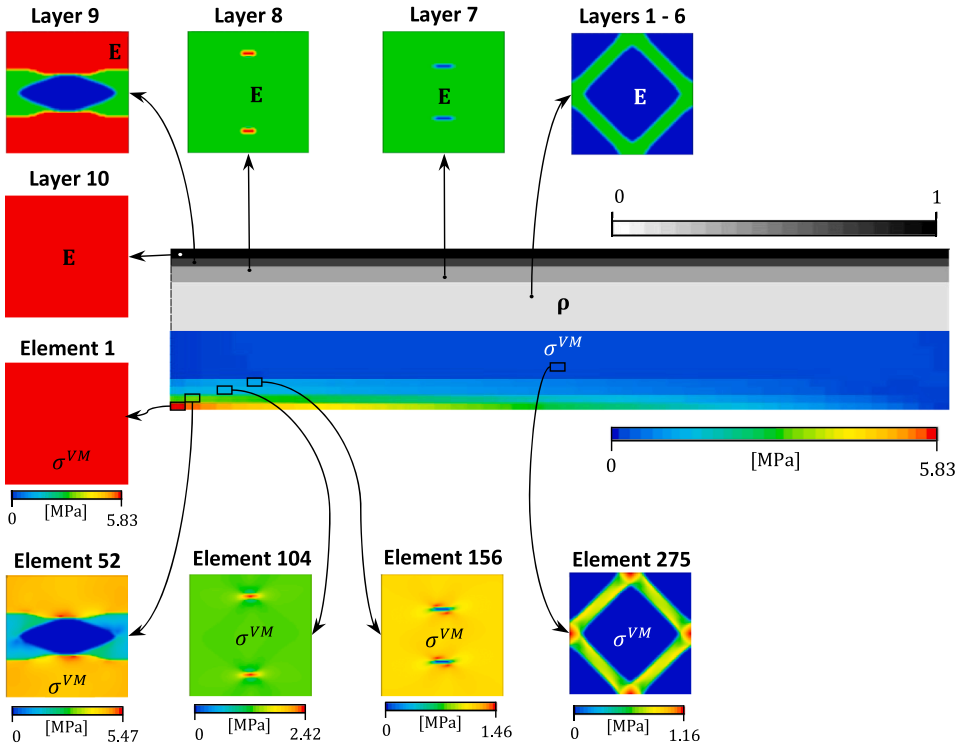

Fig. 6. LbL parametrization and non-implicit strategy (multi-scale MMTO). Optimal mass density **ρ** distribution along with the optimal multi-material micro-structures (upper half), including Von Mises stress maps (lower half).

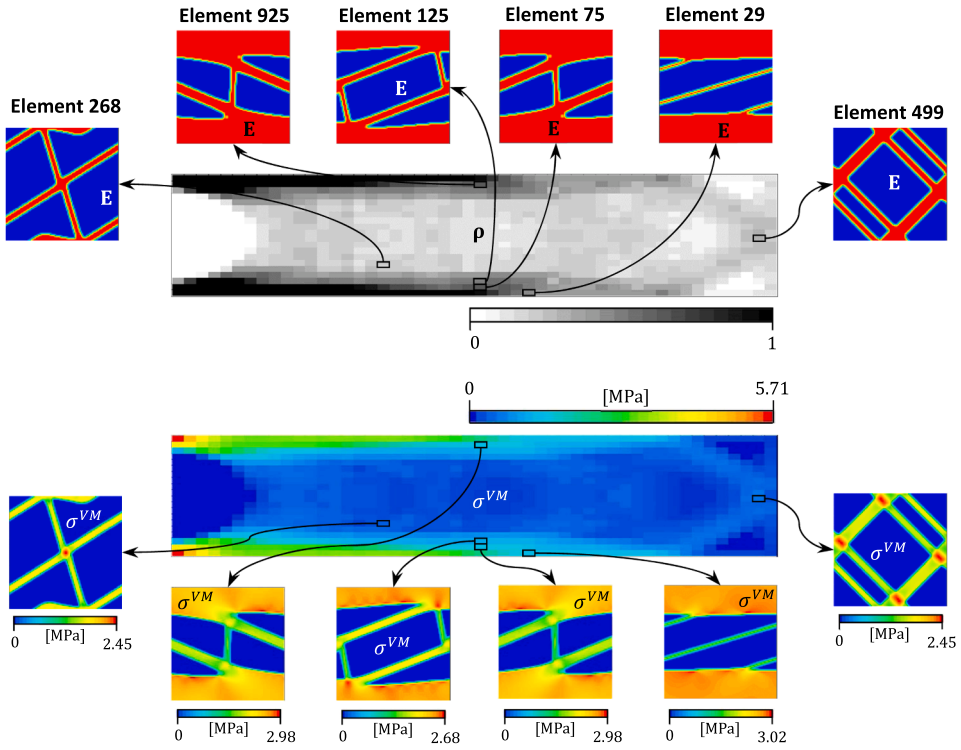

Fig. 7. EbE parametrization and non-implicit strategy (multi-scale SMTO). Optimal mass density **ρ** distribution along with a few optimal single-material micro-structures (upper half), including Von Mises stress maps (lower half).

macroscale, one optimizes the spatial distribution of mass density throughout the structure domain. Whereas, at the microscale, one optimizes the topology and material distribution (MMTO) that define each microstructure from which the structure is made of. Bearing this in mind, two coupled optimization problems are formulated, one for each scale. These can be solved using two different strategies. The *implicit* strategy assumes that the macro density design variable is implicitly computed through the micro density design variables updated by a

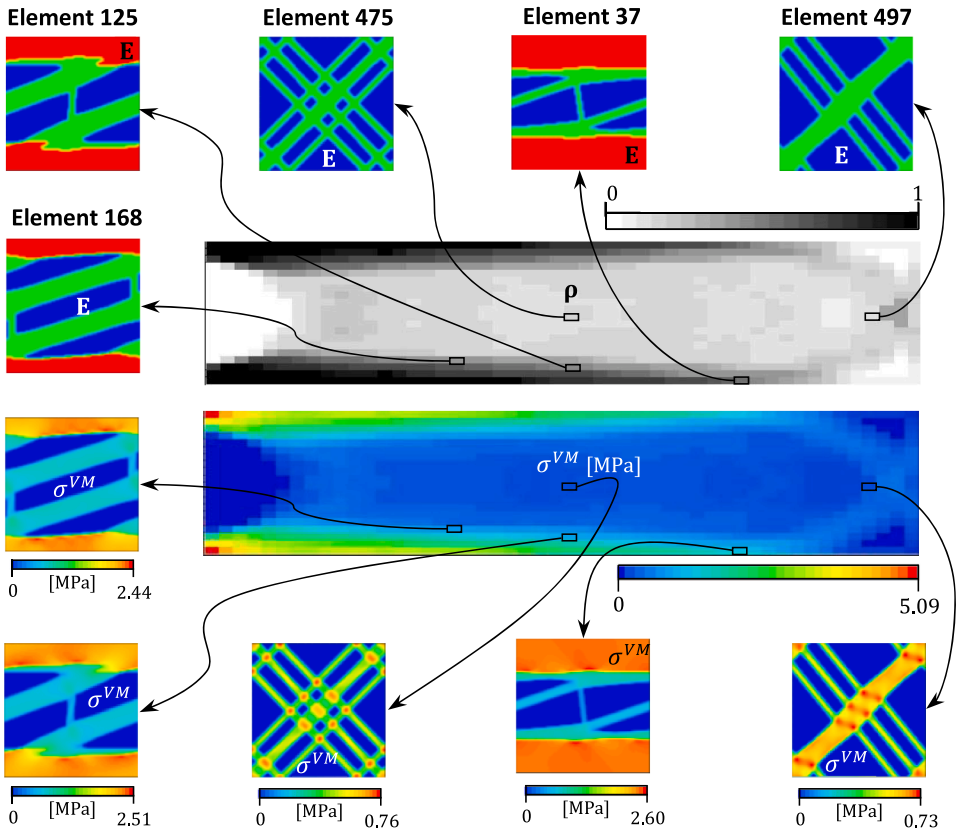

Fig. 8. EbE parametrization and non-implicit strategy (multi-scale MMTO). Optimal mass density **ρ** distribution along with a few optimal multi-material micro-structures (upper half), including Von Mises stress maps (lower half).

Table 4
Values for the total strain energy measured in Joules (C^*), total material volume fraction (V^*) and maximum Von-Mises stress in the structure measured in MPa (σ^{VM}_{max}) of the optimal SMTO and MMTO results obtained using the EbE parametrization and non-implicit strategy.

	SMTO	MMTO (δ_{SMTO})
C^*	217.40	194.78 (−10.4%)
V^*	0.30	0.55 (+83.3%)
σ^{VM}_{max}	5.71	5.09 (−10.9%)

single optimizer, while the *non-implicit* strategy assumes the macro and micro densities as independent design variables, requiring thus two optimizers working concurrently. The optimizer used here is a variant of the original MMA, called GMMA, which provides an improved approximation quality compared to the original version, since each design variable in each function is associated with its proper moving asymptote. Therefore, GMMA results in better problem convergence properties.

This work provides a comparative study between: (1) SMTO and MMTO optimal solutions; (2) two design parametrizations (LbL and EbE); and (3) two algorithmic strategies (*implicit* and *non-implicit*). Regarding the optimal solutions obtained, multi-material designs show a stiffness improvement compared to single-material ones for the same mass requirement. This is achieved on account of an increased material volume fraction. Additionally, multi-material solutions show lower stress levels when compared to single material ones, for the same loading conditions. As regards the design parameterization, the more local is the control of material microstructure the stiffer is the resulting structure, but the improved structural performance outcome comes with

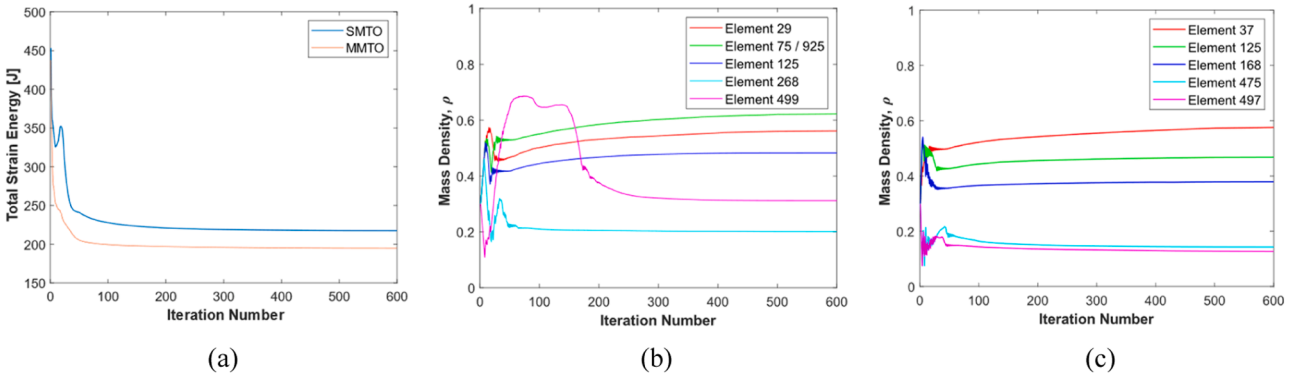

Fig. 9. Optimization history: (a) total strain energy for multi-scale SMTO and MMTO problems; (b) mass density values **ρ** for SMTO; and (c) mass density values **ρ** for MMTO.

manufacturability and computationally bigger challenges. The increased computational cost can be dealt with parallel computing using OpenMP to simultaneously tackle different micro problems on different processors. However, the scalability depends on the algorithm strategy used. The *non-implicit* strategy is more suitable to develop parallel code than the *implicit* one, therefore the former strategy is advisable for large scale multiscale TO problems. When the computational cost is not an issue, both strategies perform well, with the *implicit* one being more straightforward to be implemented.

In the future, the authors intend to extend the developed methodology to solve stress-based problems (see [57]) applied to multi-material structures, where stresses are controlled along design iterations being themselves part of the optimization problem formulation. This breakthrough is valuable since multi-material designs might not always ensure lower stress levels and, even if they do, it is not guaranteed that the yield stress of any of the materials is not exceeded. Comprehensively, this is a follow-up of much increased complexity on its own.

Declaration of Competing Interest

The authors declare that they have no known competing financial interests or personal relationships that could have appeared to influence the work reported in this paper.

Data availability

Data will be made available on request.

Acknowledgements

The authors acknowledge Fundação para a Ciência e a Tecnologia (FCT – MCTES) for its financial support through the projects UIDB/00667/2020 and UIDP/00667/2020 (UNIDEMI), UIDB/50022/2020 (IDMEC/LAETA), 2022.06903.PTDC (TOP&AM4FGM), and PhD scholarship SFRH/BD/136744/2018. Authors wish also to thank Professor Krister Svanberg (Royal Institute of Technology, Stockholm, Sweden) for the MMA optimization code.

References

[1] Aage N, Lazarov B. Parallel framework for topology optimization using the method of moving asymptotes. Struct Multidisc Optim 2013;47(4):493–505. https://doi.org/10.1007/s00158-012-0869-2.
[2] Ashby M. Materials selection in mechanical design. 4th Edition. Butterworth Heinemann; 2011. https://doi.org/10.1016/C2009-0-25539-5.
[3] Bendsøe MP, Sigmund O. Material interpolation schemes in topology optimization. Archive of Applied Mechanics 1999;69:635–54. https://doi.org/10.1007/s004190050248.
[4] Bendsøe MP, Sigmund O. Topology optimization: theory, methods and applications. Berlin: Springer; 2004. https://doi.org/10.1007/978-3-662-05086-6.
[5] Bendsøe MP. Optimal shape design as a material distribution problem. Structural Optimization 1989;1(4):193–202. https://doi.org/10.1007/BF01650949. n.
[6] Bendsøe MP, Kikuchi N. Generating optimal topologies in structural design using a homogenization method. Comput Meth Appl Mech Eng 1988;71:197–224. https://doi.org/10.1016/0045-7825(88)90086-2.
[7] Bourdin B, Chambolle A. Design-dependent loads in topology optimization. ESAIM: COCV 2003;9:19–48. https://doi.org/10.1051/cocv:2002070.
[8] Bruns T, Tortorelli D. Topology optimization of non-linear elastic structures and compliant mechanisms. Comput Meth Appl Mech Eng 2001;190(26–27):3443–59. https://doi.org/10.1016/S0045-7825(00)00278-4.
[9] Bruyneel M. SFP—A new parameterization based on shape functions for optimal material selection: application to conventional composite plies. Struct Multidisc Optim 2011;43(1):17–27. https://doi.org/10.1007/s00158-010-0548-0.
[10] Coelho P, Cardoso J, Fernandes P, Rodrigues H. Parallel computing techniques applied to the simultaneous design of structure and material. Adv Eng Software 2011;42(5):219–27. https://doi.org/10.1016/j.advengsoft.2010.10.003.
[11] Coelho P, Fernandes P, Guedes J, Rodrigues H. A hierarchical model for concurrent material and topology optimization of three-dimensional structures. Struct Multidisc Optim 2008;35(2):107–15. https://doi.org/10.1007/s00158-007-0141-3.
[12] Coelho P, Rodrigues H. Hierarchical topology optimization addressing material design constraints and application to sandwich-type structures. Struct Multidisc Optim 2015;52(1):91–104. https://doi.org/10.1007/s00158-014-1220-x.
[13] Conde FM, Coelho PG, Guedes JM. Multi-material and strength-oriented microstructural topology optimization applied to discrete phase and functionally graded materials. Struct Multidisc Optim 2022;65(4):1–22. https://doi.org/10.1007/s00158-022-03209-w.
[14] Costa MR, Sohouli A, Suleman A. Multi-scale and multi-material topology optimization of gradient lattice structures using surrogate models. Compos Struct 2022;289:115402. https://doi.org/10.1016/j.compstruct.2022.115402.
[15] Da D, Cui X, Long K, Cai Y, Li G. Multiscale concurrent topology optimization of structures and microscopic multi-phase materials for thermal conductivity. Engineering Computations 2018;36(1):126–46. https://doi.org/10.1108/EC-01-2018-0007.
[16] Da DC, Cui XY, Long K, Li GY. Concurrent topological design of composite structures and the underlying multi-phase materials. Comput Struct 2017;179:1–14. https://doi.org/10.1016/j.compstruc.2016.10.006.
[17] Dagum L, Menon R. OpenMP: an industry standard API for shared-memory programming. IEEE computational science and engineering 1998;5(1):46–55. https://doi.org/10.1109/99.660313.
[18] Deaton JD, Grandhi RV. A survey of structural and multidisciplinary continuum topology optimization: post 2000. Struct Multidisc Optim 2014;49(1):1–38. https://doi.org/10.1007/s00158-013-0956-z.
[19] Du Z, Zhou X, Picelli R, Kim HA. Connecting Microstructures for Multiscale Topology Optimization With Connectivity Index Constraints. ASME. J. Mech. Des 2018;140(11):111417. https://doi.org/10.1115/1.4041176.
[20] Fletcher R. Practical methods of optimization. John Wiley & Sons; 1987. https://doi.org/10.1002/9781118723203.
[21] Guedes J, Kikuchi N. Pre-processing and postprocessing for materials based on the homogenization method with adaptive finite element methods. Comput Meth Appl Mech Eng 1990;83(2):143–98. https://doi.org/10.1016/0045-7825(90)90148-F.
[22] Guo X, Zhang W, Zhong W. Stress-related topology optimization of continuum structures involving multi-phase materials. Comput Meth Appl Mech Eng 2014;268:632–55. https://doi.org/10.1016/j.cma.2013.10.003.
[23] Hassani B, Hinton E. A review of homogenization and topology optimization I—Homogenization theory for media with periodic structure. Comput Struct 1998;69(6):707–17. https://doi.org/10.1016/S0045-7949(98)00131-X.
[24] Hu J, Luo Y, Liu S. Two-scale concurrent topology optimization method of hierarchical structures with self-connected multiple lattice-material domains. Compos Struct 2021;272:114224. https://doi.org/10.1016/j.compstruct.2021.114224.
[25] Huang X, Zhou SW, Xie YM, Li Q. Topology optimization of microstructures of cellular materials and composites for macrostructures. Comput Mater Sci 2013;67:397–407. https://doi.org/10.1016/j.commatsci.2012.09.018.
[26] James KA. Multiphase topology design with optimal material selection using an inverse p-norm function. Int J Numer Methods Eng 2018;114(9):999–1017. https://doi.org/10.1002/nme.5774.
[27] Jia J, Cheng W, Long K, Deng H. Hierarchical design of structures and multiphase material cells. Comput Struct 2016;165:136–44. https://doi.org/10.1016/j.compstruc.2015.12.001.
[28] Jihong Z, Han Z, Chuang W, Lu Z, Shangqin Y, Zhang W. A review of topology optimization for additive manufacturing: Status and challenges. Chin J Aeronaut 2021;34(1):91–110. https://doi.org/10.1016/j.cja.2020.09.020.
[29] Kikuchi N. Finite element methods in mechanics. Cambridge: Cambridge University Press; 1986. https://doi.org/10.1017/CBO9780511569630.
[30] Lee J, Kwon C, Yoo J, Min S, Nomura T, Dede EM. Design of spatially-varying orthotropic infill structures using multiscale topology optimization and explicit de-homogenization. Additive Manufacturing 2021;40:101920. https://doi.org/10.1016/j.addma.2021.101920.
[31] Li H, Luo Z, Gao L, Walker P. Topology optimization for functionally graded cellular composites with metamaterials by level sets. Comput Meth Appl Mech Eng 2018;328:340–64. https://doi.org/10.1016/j.cma.2017.09.008.
[32] Li D, Kim IY. Multi-material topology optimization for practical lightweight design. Struct Multidisc Optim 2018;58(3):1081–94. https://doi.org/10.1007/s00158-018-1953-z.
[33] Li H, Luo Z, Xiao M, Gao L, Gao J. A new multiscale topology optimization method for multiphase composite structures of frequency response with level sets. Comput Meth Appl Mech Eng 2019;356:116–44. https://doi.org/10.1016/j.cma.2019.07.020.
[34] Liang X, Du J. Concurrent multi-scale and multi-material topological optimization of vibro-acoustic structures. Comput Meth Appl Mech Eng 2019;349:117–48. https://doi.org/10.1016/j.cma.2019.02.010.
[35] Lieu QX, Lee J. A multi-resolution approach for multi-material topology optimization based on isogeometric analysis. Comput Meth Appl Mech Eng 2017;323:272–302. https://doi.org/10.1016/j.cma.2017.05.009.
[36] Liu P, Kang Z, Luo Y. Two-scale concurrent topology optimization of lattice structures with connectable microstructures. Additive Manufacturing 2020;36:101427. https://doi.org/10.1016/j.addma.2020.101427.
[37] Liu L, Yan J, Cheng G. Optimum structure with homogeneous optimum truss-like material. Comput Struct 2008;86(13-14):1417–25. https://doi.org/10.1016/j.compstruc.2007.04.030.
[38] Moses E, Fuchs M, Ryvkin M. Topological design of modular structures under arbitrary loading. Struct Multidisc Optim 2002;24:407–17. https://doi.org/10.1007/s00158-002-0254-7.
[39] Pizzolato A, Sharma A, Maute K, Sciacovelli A, Verda V. Multi-scale topology optimization of multi-material structures with controllable geometric

complexity—Applications to heat transfer problems. Comput Meth Appl Mech Eng 2019;357:112552. https://doi.org/10.1016/j.cma.2019.07.021.
[40] Rodrigues H, Guedes JM, Bendsøe MP. Hierarchical optimization of material and structure. Struct Multidisc Optim 2002;24(1):1–10. https://doi.org/10.1007/s00158-002-0209-z.
[41] Sigmund O. Morphology-based black and white filters for topology optimization. Struct Multidisc Optim 2007;33:401–24. https://doi.org/10.1007/s00158-006-0087-x.
[42] Sivapuram R, Dunning PD, Kim HA. Simultaneous material and structural optimization by multiscale topology optimization. Struct Multidisc Optim 2016;54(5):1267–81. https://doi.org/10.1007/s00158-016-1519-x.
[43] Sokolowski J, Zochowski A. On the Topological Derivative in Shape Optimization. SIAM J Control Optim 1999;37(4):1251–72. https://doi.org/10.1137/S0363012997323230.
[44] Stegmann J, Lund E. Discrete material optimization of general composite shell structures. Int J Numer Methods Eng 2005;62(14):2009–27. https://doi.org/10.1002/nme.1259.
[45] Svanberg K. The method of moving asymptotes - a new method for structural optimization. Int J Numer Methods Eng 1987;24(2):359–73. https://doi.org/10.1002/nme.1620240207.
[46] Swan CC, Arora JS. Topology design of material layout in structured composites of high stiffness and strength. Structural Optimization 1997;13:45–59. https://doi.org/10.1007/BF01198375.
[47] Tavakoli R, Mohseni SM. Alternating active-phase algorithm for multimaterial topology optimization problems: a 115-line MATLAB implementation. Struct Multidisc Optim 2014;49:621–42. https://doi.org/10.1007/s00158-013-0999-1.
[48] Wang Y, Chen F, Wang MY. Concurrent design with connectable graded microstructures. Comput Meth Appl Mech Eng 2017;317:84–101. https://doi.org/10.1016/j.cma.2016.12.007.
[49] Wang MY, Wang X. Color" level sets: a multi-phase method for structural topology optimization with multiple materials. Comput Meth Appl Mech Eng 2004;193(6–8):469–96. https://doi.org/10.1016/j.cma.2003.10.008. n.
[50] Wang MY, Wang X, Guo D. A level set method for structural topology optimization. Comput Meth Appl Mech Eng 2003;192(1-2):227–46. https://doi.org/10.1016/S0045-7825(02)00559-5.
[51] Wu J, Sigmund O, Groen JP. Topology optimization of multi-scale structures: a review. Struct Multidisc Optim 2021;63(3):1455–80. https://doi.org/10.1007/s00158-021-02881-8.
[52] Xu B, Jiang JS, Xie YM. Concurrent design of composite macrostructure and multi-phase material microstructure for minimum dynamic compliance. Compos Struct 2015;128:221–33. https://doi.org/10.1016/j.compstruct.2015.03.057.
[53] Yin L, Ananthasuresh GK. Topology optimization of compliant mechanisms with multiple materials using a peak function material interpolation scheme. Struct Multidisc Optim 2001;23:49–62. https://doi.org/10.1007/s00158-001-0165-z.
[54] Zhang WH, Fleury C, Duysinx P, Nguyen VH, Laschet I. A generalized method of moving asymptotes (GMMA) including equality constraints. Structural optimization 1996;12(2):143–6. https://doi.org/10.1007/BF01196948.
[55] Zhang Y, Xiao M, Li H, Gao L, Chu S. Multiscale concurrent topology optimization for cellular structures with multiple microstructures based on ordered SIMP interpolation. Comput Mater Sci 2018;155:74–91. https://doi.org/10.1016/j.commatsci.2018.08.030.
[56] Zhao L, Xu B, Han Y, Rong J. Concurrent design of composite macrostructure and cellular microstructure with respect to dynamic stress response under random excitations. Compos Struct 2021;257:113123. https://doi.org/10.1016/j.compstruct.2020.113123.
[57] Zhao R, Zhao J, Wang C. Stress-constrained concurrent topology optimization of two-scale hierarchical structures. Int J Numer Methods Eng 2021;122(21):6126–54. https://doi.org/10.1002/nme.6785.
[58] Zhou S, Wang MY. Multimaterial structural topology optimization with a generalized Cahn-Hilliard model of multiphase transition. Struct Multidisc Optim 2007;33:89–111. https://doi.org/10.1007/s00158-006-0035-9.
[59] Zhou XY, Du Z, Kim HA. A level set shape metamorphosis with mechanical constraints for geometrically graded microstructures. Struct Multidisc Optim 2019;60(1):1–16. https://doi.org/10.1007/s00158-019-02293-9.
[60] Zuo W, Saitou K. Multi-material topology optimization using ordered SIMP interpolation. Struct Multidisc Optim 2017;55(2):477–91. https://doi.org/10.1007/s00158-016-1513-3.